Effect of future $B_c \to \tau\nu_\tau$ measurements to constrain new physics in the $b \to c\ell\nu_\ell$ transition.

author: M.J. Sikkens
Supervisor: dr. K.A.M. de Bruyn

July 24, 2025

Abstract

Anomalies in semileptonic B meson decays—particularly in the observables $R(D)$ and $R(D^*)$—suggest possible violations of lepton flavour universality and point toward physics beyond the Standard Model (SM). In this thesis, I investigate the potential of the purely leptonic decay $B_c \to \tau\nu$ to further constrain New Physics (NP) contributions in the transition $b \to c\ell\nu$ within the framework of Effective Field Theory (EFT).

I build upon the framework created by R. Fleischer and others, using a complete basis of dimension-6 operators, and focus on scenarios involving pseudoscalar and left-handed vector operators, motivated by their direct contributions to the observables under study.

A global fit is performed using the `GammaCombo` fitting framework which includes the latest measurements of $R(D)$, $R(D^*)$, $R_{e/\mu}$, and $F_L(D^*)$, along with the SM prediction and projected experimental uncertainty for a $\mathcal{B}(B_c \to \tau\nu)$ measurement at LHCb.

The inclusion of $B_c \to \tau\nu$ significantly improves constraints on the pseudoscalar Wilson coefficient $C_P^{c,\tau}$, reducing the allowed parameter space by a factor of approximately 6.6. In multi-parameter scenarios, it provides a complementary constraint where other observables fail to do so. These results demonstrate the crucial role of leptonic decays in shaping model-independent bounds on NP contributions and emphasize the importance of future experimental measurements of $B_c \to \tau\nu$ for resolving current tensions in flavour physics.

Contents

1 Introduction

Curiosity lies at the very heart of physics. The pursuit of fundamental questions about the universe drives the development of experiments, observations, and theories. Throughout the last century, theory and experiments have pushed each other to discoveries. Around 1960, many particles were found that were thought to be elementary. Nowadays, these particles are known as hadrons that are composed of multiple elementary particles called quarks. Together with the other known elementary particles called leptons, containing the electron, muon, tau, and their respective neutrinos, these discoveries culminated in the formulation of a comprehensive theoretical framework: the Standard Model (SM) of particle physics [1]. The Standard Model successfully describes the known fundamental particles and their interactions, with the notable exception of gravity.

Not only did the SM successfully account for the particles known at that time, but it also predicted the existence of new ones. In 1973, Kobayashi and Maskawa [2] proposed an extension to the four-quark model at the time to describe CP violation. Later in 1977 and 1995 the bottom quark[3] and top quark[4, 5], respectively, were found to complete the quark sector of the SM. The Higgs discovery in 2012 by the ATLAS[6] and CMS collaborations [7] at the Large Hadron Collider (LHC) marked a major triumph for the SM and completed the model's particle content.

Despite this success, there remain strong indications that the SM is not the ultimate theory of fundamental interactions but an approximation to a more complete theory. Experimental anomalies such as dark matter[8] and matter/antimatter asymmetry suggest the existence ofphysics beyond the Standard Model (BSM) as they can not be explained by the framework of the SM today. Many experiments have tested the properties of the SM, and I will focus on Lepton Flavour Universality (LFU). The Standard Model states that all leptons are treated equally except for a difference in mass. Yet experiments [9, 10, 11] found signs of Lepton Flavour Universality Violation (LFUV) in

$$\mathcal{R}(D^{(*)}) = \frac{\mathcal{B}r(\bar{B} \to D^{(*)}\tau\nu_\tau)}{\mathcal{B}r(\bar{B} \to D^{(*)}\ell'\nu_{\ell'})}, \quad \ell' = (e, \mu). \tag{1}$$

Where $R(D^{(*)})$ describes the ratio of branching fractions of similar semileptonic decays of mesons consisting of an anti-bottom quark and an up or down quark and/or their conjugate particles, by the quark level process $b \to c\ell\nu_\ell$ where $\ell = (e, \mu, \tau)$. For simplicity I will not distinguish between matter and anti-matter, reactions will be generalized if possible. In the 2D plane $R(D)$ and $R(D^*)$ show a tension larger than 3σ [12] with the SM (figure 1), making it an interesting probe for BSM physics.
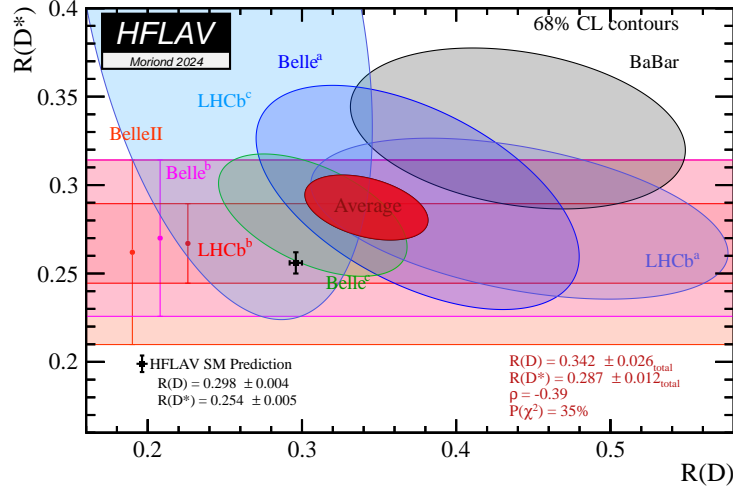
Figure 1: Two dimensional display of the different measurements of $R(D)$ and $R(D^*)$. The world average is shown in red and the SM prediction in black.

The search for physics BSM has been ongoing, with the one of the main facilities being the LHC located at CERN. By colliding high-energy protons with each other, Center of mass energy collisions exceeding 13TeV form an environment able to create heavier particles. Current measurements [13, 14] show no evidence of new particles below a mass of 1TeV. As this mass is much higher than the energies considered in $b \to c\ell\nu_\ell$ transitions, it is possible to create a framework including NP without needing a full high energy theory using Effective Field Theory (EFT).

EFT allows for a complete view on NP, where processes are treated as contact interaction. In such contact interactions, complicated kinematics of mediating (new) heavy particles are included in one or multiple operators. The coupling strength of these operators is given by their corresponding Wilson coefficients. The strength of EFT lies in the Operator Product Expansions (OPEs), where all processes have a dependence on (multiple) Wilson coefficients. In general, there are too many Wilson coefficient dependencies, but with enough measurements and the right assumptions, it is possible to constrain the space for NP by constraining the Wilson coefficients.

I will follow the approach of R. Fleischer et al. [15] to constrain NP Wilson coefficients of $b \to c\ell\nu_\ell$ operators and continue by adding the branching fraction of the $B_c \to \tau\nu_\tau$ decay, which the LHCb group in Groningen is trying to measure. $B_c \to \tau\nu_\tau$ follows the $b \to c\ell\nu_\ell$ like the decays in $R(D)$ and $R(D^*)$ but has no hadron in the final state. The main questions of this thesis will be how this measurement will affect the constraints on the Wilson coefficients

2 Theory

[1] In the theory section, I will introduce the different concepts needed in order to follow the analysis. Starting with an overview of the Standard Model and the concepts needed for (Semi-)leptonic meson decays. After the introduction of the Standard Model, the motivation for this analysis is expanded to include these concepts. When the SM and the motivation are clear, Effective field theory is introduced with an eye on the $b \to c\ell\nu_\ell$ transition as a basis for the framework in the analysis.

2.1 Standard Model

The Standard Model describes two things: What elementary particles exist and the rules between them. First, I will give an overview of these particles and rules, and after using them to explain how hadron decays can be used to test the SM. With that information, I will give more context to the motivation for this thesis.
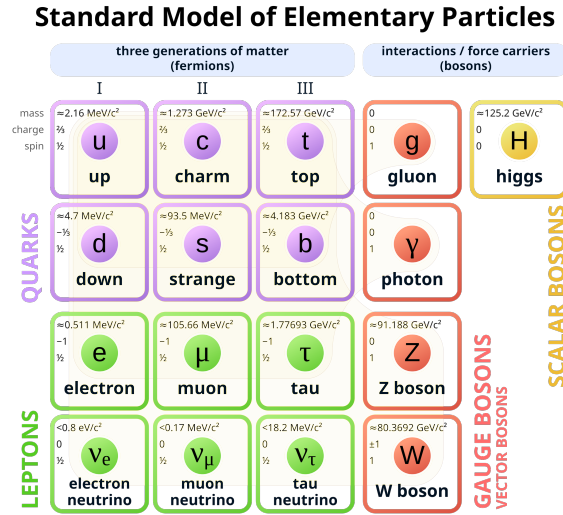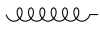
Figure 2: Complete particle content of the Standard Model of particle physics

Gauge bosons in the Standard Model

Strong interaction

The strong interaction acts on particles carrying color charge. It is mediated by eight massless gauge bosons called gluons. This force binds quarks into hadrons and exhibits the property of confinement, which prevents isolated quarks from being observed. The strong force is the most powerful of the three SM interactions, with a relative strength of order unity at typical hadronic scales.

---

[1]For this section ChatGPT-4[16] has been used as a writing tool

Electromagnatic interaction

The electromagnetic interaction governs the behavior of electrically charged particles. It is mediated by the massless photon and conserves electric charge. At low energies, its strength is quantified by the fine-structure constant $\alpha \approx 1/137$. While weaker than the strong force, the electromagnetic interaction has an infinite range and plays a dominant role in atomic and molecular phenomena.

Weak interaction

The weak interaction acts on the weak isospin; this interaction is mediated by the massive W^+, W^-, and Z^0 bosons. The weak force is unique in that it only couples to left-handed fermions and is capable of changing the flavour(type) of quarks and leptons. Its short range and apparent weakness compared to the strong and electromagnetic forces arise primarily due to the large masses of its mediating bosons, leading to a suppression by a factor of roughly 10^{-6} in typical low-energy processes.

Fermions in the Standard Model

Fermions are the fundamental building blocks of matter. In the Standard Model, they are organised into two main groups: leptons and quarks. Each group comes in three generations of increasing mass and similar quantum numbers. These fermions are subject to the gauge interactions described earlier, depending on their charges under the relevant symmetry groups.

Each generation includes two types of leptons and two types of quarks, arranged in weak isospin doublets. The left-handed components of these fermions transform as doublets under $SU(2)_L$, while their right-handed components are singlets and do not participate in charged weak interactions. This chiral structure of the Standard Model is a defining feature, particularly in weak processes, where only left-handed fermions and right-handed antifermions interact via the W bosons.

Leptons

Leptons are electrically charged or neutral particles that do not carry colour charge and therefore do not participate in the strong interaction. Each generation consists of a charged lepton—electron (e), muon (μ), or tau (τ)—and its corresponding neutrino (ν_e, ν_μ, ν_τ). Charged leptons interact via both the electromagnetic and weak forces, while neutrinos interact only weakly. In the Standard Model, neutrinos are massless, although experimental observations of neutrino oscillations indicate that this assumption is incomplete and that neutrinos must possess small, non-zero masses.

Quarks

Quarks are fermions that carry both electric charge and colour charge, allowing them to participate in all three Standard Model interactions: strong, weak, and electromagnetic. They come in six flavours, organised into three generations: up (u) and down (d), charm (c) and strange (s), top (t) and bottom (b). Up-type quarks (u, c, t) carry a charge of $+2/3$, while down-type quarks (d, s, b) carry a charge of $-1/3$. Due to colour confinement, quarks are never observed in isolation but bind together to form colour-neutral hadrons, such as mesons (quark–antiquark pairs) and baryons

(three-quark states).

The quark sector plays a crucial role in flavour physics, particularly in the context of weak decays, where transitions between different quark flavours occur via the charged current interactions. These transitions are governed by the Cabibbo–Kobayashi–Maskawa (CKM) matrix, which will be discussed in detail in the next section.

Quark Mixing and the CKM Matrix

In the Standard Model, weak interactions mediated by the $W^{\pm}$ bosons are responsible for transitions between different quark flavours. These transitions occur only among the $SU(2)_L$ doublets. However, the weak eigenstates of the down-type quarks (d, s, b) do not coincide with their corresponding mass eigenstates. This misalignment leads to flavour mixing in the charged current interactions and is described by the CKM matrix [17, 18].

The CKM matrix, denoted by V_{CKM}, is a unitary 3×3 matrix that relates the weak interaction eigenstates of the down-type quarks to their mass eigenstates:

$$\begin{pmatrix} d' \\ s' \\ b' \end{pmatrix} = V_{\text{CKM}} \begin{pmatrix} d \\ s \\ b \end{pmatrix}, \tag{2}$$

where the primed fields are weak eigenstates and the unprimed fields are mass eigenstates. The CKM matrix elements V_{ij} quantify the strength of the charged current interaction between an up-type quark $i = u, c, t$ and a down-type quark $j = d, s, b$.

This flavour mixing allows for processes in which the flavour of a quark changes through the emission or absorption of a $W^{\pm}$ boson, referred to as flavour-changing charged currents (FCCC). Semileptonic and leptonic decays of B mesons, such as $B \to D^{(*)}\ell\nu_\ell$ and $B_c \to \tau\nu_\tau$, proceed via the quark-level transition $b \to c\ell\nu_\ell$. These transitions are proportional to the CKM matrix element $|V_{cb}|$. A longstanding issue in the determination of $|V_{cb}|$ is the discrepancy between values obtained from inclusive and exclusive measurements [12].

$$\begin{aligned} |V_{cb}|_{\text{incl.}} &= (42.2 \pm 0.5) \times 10^{-3} \\ |V_{cb}|_{\text{excl.}} &= (39.8 \pm 0.6) \times 10^{-3} \end{aligned} \tag{3}$$

Inclusive determinations, based on the total semileptonic decay rate of $B \to X_c \ell\nu_\ell$, where X_c denotes any charmed hadronic final state, tend to yield higher values of $|V_{cb}|$ compared to exclusive determinations using specific decay modes such as $B \to D\ell\nu_\ell$ or $B \to D^*\ell\nu_\ell$ [12]. The difference between these methods is around 3 sigma and remains unresolved despite advances in theoretical treatments, including heavy quark effective theory, lattice QCD calculations of form factors [19], and improved experimental measurements. This tension complicates global fits of the CKM matrix and raises the question of whether new physics contributions could be affecting one or both types of determinations.

The value of V_{cb} plays a crucial role in determining theoretical predictions for branching ratios and differential decay rates of semileptonic and leptonic B decays. Accurate measurements of these

observables therefore not only test the structure of the SM but also provide constraints on the magnitude of V_{cb}. Deviations from the Standard Model predictions, particularly in decay channels involving the τ lepton, may indicate new physics contributions, such as additional operators arising from physics beyond the Standard Model. In this context, the study of FCCC processes in b-quark meson decays becomes a powerful probe of both the SM and its possible extensions.

2.1.1 Lepton flavour universality

The SM assumes that all leptons couple identically to the weak interaction, a principle known as lepton flavour universality, this is a cornerstone of the SM. Deviations from this assumption, known as lepton flavour universality violation , are therefore promising indicators of new physics. Measurements of semileptonic B meson decays — particularly those involving τ leptons (figure 3a) — have shown tensions with SM predictions, suggesting possible LFUV. key observables in this context are the two branching fraction ratios,

$$R(D^{(*)}) = \frac{\mathcal{B}r(B \to D^{(*)}\tau\nu_\tau)}{\mathcal{B}r(B \to D^{(*)}\ell'\nu_{\ell'})} \quad (\ell' = e, \mu).$$

which together are in tension with the SM[12] (figure 1). While no single measurement is in tension with the SM, the average of all these measurements shows an average outside of the SM at 3 sigma.

A compelling feature of semileptonic B-meson decays is that have with sufficient mass to produce the heavy τ lepton in the final state. This makes them an essential probe for testing LFU as all lepton generations can be involved. Observables involving $b \to c\ell\nu_\ell$ transitions, such as the ratios $R(D^{(*)})$, are thus powerful tools in the search for violations of LFU and, consequently, hints of physics beyond the Standard Model. The leptonic $B_c^+ \to \tau^+\nu_\tau$ decay(figure 3b) also follows the $b \to c\ell\nu_\ell$ transition but does not have a meson in the final state. This decay has not been measured yet but is currently being investigated by the LHCb experiment.
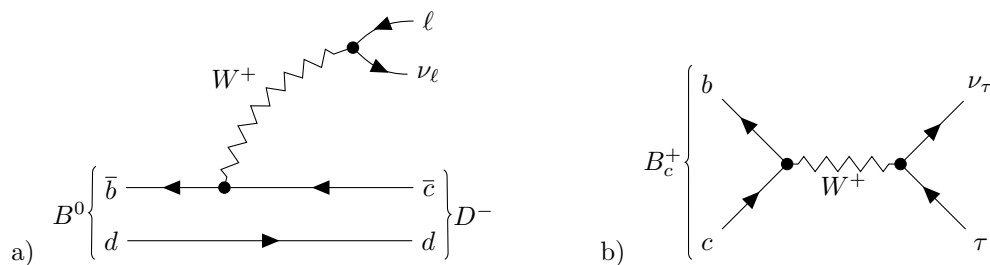

Figure 3: Feynman diagrams of the leading order $B^0 \to D^-\ell\nu_\ell$ and $B_c^+ \to \tau^+\nu_\tau$ decay

However, the production and study of heavy particles such as B mesons — and especially B_c mesons — come with experimental challenges. At electron-positron (e^+e^-) colliders like Belle II, B-meson pairs are produced in a clean environment through the $\Upsilon(4S)$ resonance, yielding neutral $(B^0\bar{B}^0)$ or charged (B^+B^-) meson pairs. These facilities allow for precision studies of B mesons with minimal background interference. While higher-energy e^+e^- collisions can produce $B_s\bar{B}_s$ pairs through the $\Upsilon(5S)$ resonance, they do not efficiently yield B_c mesons due to phase-space limitations

and the requirement for both a b and a c quark in the initial state.

To study decays of the B_c meson, one must turn to hadron colliders, such as the (LHC). In this environment, the LHCb experiment is specifically optimized for studying heavy-flavour hadrons and is currently the primary source of experimental data on B_c decays. Despite the more complex collision environment and higher backgrounds, hadron colliders offer access to a wider variety of heavy meson states, including those crucial for probing $b \to c\tau\nu_\tau$ transitions.

2.2 Effective Field Theory

This section will introduce the necessary context on Effective Field Theory for this thesis. Starting with a general introduction and historical context to show its versatility. Next, the potential operators are introduced together with their Wilson coefficients and how they incorporate new physics. Last the framework, that has been provided by [15] is explained in this context.

2.2.1 Fermi

A classic example of an effective field theory is Fermi's theory of beta decay, formulated in the 1930s [20]. In beta decay, a neutron transforms into a proton, emitting an electron and an antineutrino (figure 4a). Fermi proposed that this process could be described by a contact interaction involving four fermions at a single spacetime point, characterized by the effective Lagrangian:

$$\mathcal{L}_{\text{Fermi}} = -G_F \left(\bar{p}\gamma^\mu n\right)\left(\bar{e}\gamma_\mu \nu_e\right) + \text{h.c.} \tag{4}$$

where G_F is the Fermi coupling constant, p and n are the proton and neutron fields, and e and ν_e are the electron and electron neutrino fields, respectively.

At the time, the mediators of the weak force (the $W^\pm$ bosons) were unknown. Fermi's theory successfully described weak interactions at low energies without invoking any underlying mediating particles. It was later understood that Fermi's contact interaction is the low-energy limit of the exchange of a massive W boson (figure 4b), with the Fermi constant related to the weak coupling and the mass of the W boson by:

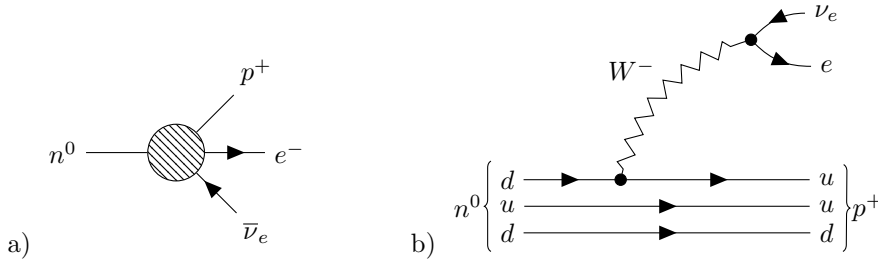$$G_F = \frac{\sqrt{2}g^2}{8M_W^2} \tag{5}$$

Figure 4: Showing the beta-decay process of a neutron decaying into a proton, an electron and an anti electron neatrino. The left Diagram shows an EFT view, where the underlying process is unknown. The right diagram shows the 1st order SM contribution, with the mediating W boson.

This historical example highlights the power of effective field theories: they allow for accurate and predictive modeling of unknown high-energy physics in terms of low-energy observables. Similarly, modern applications of EFT aim to capture the effects of heavy NP particles on experimentally accessible processes, even if direct production of the new particles is beyond current experimental reach.

The next section will describe an EFT for the $b \to c\ell\nu_\ell$ transition and highlight both the strengths and shortcomings of such an approach to find NP.
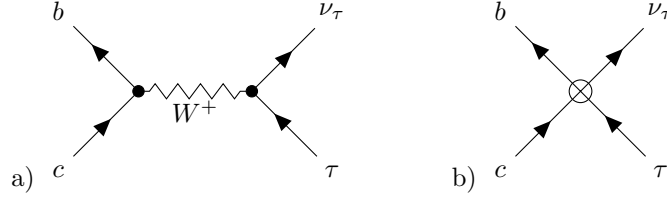
2.2.2 EFT for $b \to c\ell\nu_\ell$

Figure 5: The left diagram shows the full SM tree-level decay mediated by the W boson, while the right diagram shows the point interaction described by EFT

Based on [15], we now apply the EFT formalism to the quark-level transition $b \to c\ell\nu_\ell$. In the SM, this process is mediated by a tree-level W boson exchange (figure 5a), which in the EFT formalism is described by an effective four-fermion interaction (figure 5b) with the following Hamiltonian,

$$\mathcal{H}_{\text{eff}} = \frac{4G_F}{\sqrt{2}} V_{cb} \sum_i \tilde{C}_i^{c,\ell} \, \mathcal{O}_i^{c,\ell}. \tag{6}$$

where $\mathcal{O}_i^{c,\ell}$ are dimension-six operators built from quark and lepton fields, and the Wilson coefficients, $C_i^{c,\ell}$, encode the short-distance physics. ℓ sums over the lepton flavours (e, μ, τ) and i sums over the relevant operators in $b \to c\ell\nu_\ell$ transitions,

$$\mathcal{O}_{V_L}^{c,\ell} = (\bar{c}\gamma^\mu P_L b)(\bar{\ell}\gamma_\mu P_L \nu_\ell), \tag{7}$$

$$\mathcal{O}_{V_R}^{c,\ell} = (\bar{c}\gamma^\mu P_R b)(\bar{\ell}\gamma_\mu P_L \nu_\ell), \tag{8}$$

$$\mathcal{O}_{S}^{c,\ell} = \frac{1}{2}(\bar{c}b)(\bar{\ell}P_L \nu_\ell), \tag{9}$$

$$\mathcal{O}_{P}^{c,\ell} = \frac{1}{2}(\bar{c}\gamma^5 b)(\bar{\ell}P_L \nu_\ell), \tag{10}$$

$$\mathcal{O}_{T}^{c,\ell} = (\bar{c}\sigma^{\mu\nu} P_L b)(\bar{\ell}\sigma_{\mu\nu} P_L \nu_\ell). \tag{11}$$

Where γ^μ are the gammma matrixes, $\gamma^5 = \gamma^0\gamma^1\gamma^2\gamma^3$ is used to separate left and right chirality and $P_{L,R} = (1 \mp \gamma^5)$. $\mathcal{O}_{V_L}^{c,\ell}$ is the left-handed vector operator and is the only operator contributing to the SM, the other operators contribute to BSM interactions. $\mathcal{O}_{V_R}^{c,\ell}$ is the right-handed vector operator and describes a flavour-changing vector current coupling to right-handed fermion fields. $\mathcal{O}_{S}^{c,\ell}$, $\mathcal{O}_{P}^{c,\ell}$, and $\mathcal{O}_{T}^{c,\ell}$ describe the scalar, pseudoscalar and tensor operators respectively. While the SM does

contain a scalar interaction with the Higgs boson,$\mathcal{O}_S^{c,\ell}$ and $\mathcal{O}_P^{c,\ell}$ are BSM because the Higgs boson can't change flavour. Tensor interactions are not described by the SM.

In order to find contributions to NP, the Wilson Coefficients can be decomposed into their SM and NP value.

$$\tilde{C}_i^{c,\ell} = C_i^{c,\ell(\text{SM})} + C_i^{c,\ell(\text{NP})} \tag{12}$$

As $\mathcal{O}_{V_L}^{c,\ell}$ contributes to the SM, its Wilson coefficient SM contribution is set to 1. The other operators do not contribute to the SM, and their SM contribution will vanish, i.e.

$$C_{V_L}^{(\text{SM})c,\ell} = 1, \qquad C_{VR}^{(\text{SM})c,\ell} = C_S^{(\text{SM})c,\ell} = C_P^{(\text{SM})c,\ell} = C_T^{(\text{SM})c,\ell} = 0 \tag{13}$$

Notice how the coefficients are general for the leptons in eq 6 ,$\ell = \{e, \mu, \tau\}$, where for the different lepton flavours the Wilson coefficients will generally have different values and must all be fitted. The total number of Wilson coefficients for this transition becomes 13. $C_{V_R}^c$ assumes LFU and is equal for all leptons, decreasing the total by 2. This showcases one of the difficulties of EFT, the large number of Wilson coefficients makes it difficult to find a solution for all Wilson coefficients at once. In order to limit the degrees of freedom, I made the following assumptions about the Wilson coefficients. I assume NP to be CP conserving, this reduces the Wilson coefficients to real numbers only instead of the general complex Wilson Coefficients. Second, I will assume a relation between the electron and Muon Wilson coefficient,

$$C_i^{c,e} = f_\mu^e C_i^{c,\mu} \tag{14}$$

where f_μ^e is a constant and follow the same scenarios as [15].

$$\begin{aligned} f_\mu^e &= 0.1, & C_i^{c,e} &> C_i^{c,\mu} \\ f_\mu^e &= 1, & C_i^{c,e} &\approx C_i^{c,\mu} \\ f_\mu^e &= 10, & C_i^{c,e} &< C_i^{c,\mu} \end{aligned} \tag{15}$$

And last, I will only look two Wilson coefficients at the time. Either for pseudoscalar or left handed vector Wilson coefficients of all lepton generations using the relations described above, or by looking at pseudoscalar and left handed vector Wilson coefficients of only tau leptons. This way the observables will always be able to find bound constraints.

B meson decays happen at the energy scale of the b quark mass ($m_b = 4.183 \pm 0.004\ GeV$[21]), while the energy scale for NP is considered to be of 1 TeV or higher[14, 13]. Wilson Coefficients are general dependent on the energy scale of the processes. In order to describe the Wilson coefficients at the NP scale (1 TeV) where we expect a potential new particle to be, the equations [15, 22]

$$\begin{aligned} C_P^{c,\ell}(m_b) &= 1.71 C_P^{c,\ell}(1\ TeV), \\ C_{V_L}^{c,\ell}(m_b) &= C_{V_L}^{c,\ell}(1\ TeV). \end{aligned} \tag{16}$$

show how the pseudoscalar and left handed vector transform between different energy scales.

3   Methods

This section will provide the analysis in this thesis. First, all observables used together with their measurement and SM values are listed, as well as the predicted Branching fraction of $B_c \rightarrow$

$\tau\nu_\tau$. After, I will show how these observables depend on the Wilson coefficients and how these dependencies can be derived. And finally the fitting strategy is described where the measurement and WC dependency are put together

3.1 Observables

Thus far, we have introduced the $R(D^{(*)})$ discrepancy and how it shows hints towards LFUV. This measurement alone is not enough to find precise constraints on the Wilson coefficients. Therefore I will follow the approach in [15] and add the following observables to our analysis,

$$\mathcal{R}_\mu^e(D^*) = \frac{\mathcal{B}r(B^0 \to D^{*-}e^+\nu_e)}{\mathcal{B}r(B^0 \to D^{*-}\mu^+\nu_\mu)}$$
$$F_L(D^*) = \frac{\Gamma(B^0 \to D_L^{*-}\tau^+\nu_\tau)}{\Gamma(B^0 \to D^{*-}\tau^+\nu_\tau)} \tag{17}$$

where $\mathcal{R}_\mu^e(D^*)$ is a ratio of branching fractions of $B^0 \to D^{*-}\ell'^+\nu_{\ell'}$ decays for $\ell' = \{e, \mu\}$. $F_L(D^*)$ looks at the longitudinal polarization of the D^* meson after the decay. Together, they are dependent on each Wilson coefficient relevant to the $b \to c\ell\nu_\ell$ transition. Table 1 gives an overview of the measurements that are used in this thesis, the vlaues have not changed much since [15] in 2021. The one notable difference is a new measurement of $F_L(D^*)$ by LHCb[23] differing 1.5 sigma from the previous $0.60 \pm 0.08 \pm 0.04$[24] . In order to find the relative contribution from NP Wilson coefficient to SM, the measurements are normalized using their SM values.
To explore the impact of a future measurement, I have added the SM value for the not yet measured branching fraction,

$$\mathcal{B}r(B_c \to \tau\nu_\tau) \tag{18}$$

where with the use of [25], studying the feasibility for finding this decay, I was able to get a estimate for the projected uncertainty of the branching fraction using LHCb run 3 data.

$$\mathcal{B}(B_c^+ \to \tau^+\nu_\tau)/\mathcal{B}(B_c^+ \to \tau^+\nu_\tau)^{SM} = 1.00 \pm 0.32 \tag{19}$$

Observable	Experiment	SM(theory)	SM ratio
$F_L(D^*)$	$0.43 \pm 0.06 \pm 0.03$ [23]	0.458 ± 0.004 [15]	0.94 ± 0.15
$R(D)$	0.342 ± 0.026 [26]	0.298 ± 0.004 [26]	1.15 ± 0.09
$R(D^*)$	0.287 ± 0.012 [26]	0.254 ± 0.005 [26]	1.13 ± 0.06
$\mathcal{R}_\mu^e(D^*)$	$1.01 \pm 0.01 \pm 0.03$ [27]	$1.0045(1)$ [15]	1.005 ± 0.032

Table 1: Table with the measured observables used to constrain the Wilson coefficients together with their SM predictions. The last column shows the ratio between experiment and SM prediction

3.2 Wilson coefficient relations

This section will show how to derive the WC dependencies for the different processes through the Effective amplitudes. For most processes, this comes down to large calculations with many parameters that will not add clarity for this thesis. That is why I will show the steps to get an OPE for the simplest case, an annihilation decay, $B_c \to \tau\nu_\tau$. This decay is theoretically clean in de sense that there are no hadrons in the decay products, and it being a 2-body decay, making the kinematics much simpler.

Leptonic ($B_c \to \tau\nu_\tau$)

In order to get the effective amplitude you have to take the following product

$$\mathcal{A}(i \to f) = \langle f|\mathcal{H}|i\rangle \tag{20}$$

Because this section is more about the structure of the Wilson coefficients as opposed to a quantum field theory course, I will skip most steps of the calculation. For the $B_c \to \tau\nu_\tau$ decay, the effective amplitude becomes

$$\mathcal{A}(B_c \to \tau\nu) = \frac{G_F}{\sqrt{2}} V_{cb} f_{B_c} \; (\bar{\tau} P_L \nu_\tau) \left[(1 + C_{V_L}^{c,\tau}) m_\tau + \frac{m_{B_c}^2}{m_b + m_c} C_P^{c,\tau} \right]. \tag{21}$$

Where $(\bar{\tau} P_L \nu_\tau)$ describes the leptonic creation and the Wilson coefficients show the NP contributions. When the Wilson coefficients are set to zero, the remaining amplitude is the low-energy limit of the SM.

With this Amplitude, it is possible to compute observables like the branching fraction

$$\mathcal{B}r(B_c \to \tau\nu_\tau) = \mathcal{B}r(B_c \to \tau\nu_\tau)^{\mathrm{SM}} \left| 1 + C_{V_L} + \frac{m_{B_c}^2}{m_\tau (m_b + m_c)} C_P \right|^2, \tag{22}$$

where

$$\mathcal{B}r(B_c \to \tau\nu_\tau)^{\mathrm{SM}} = \frac{G_F^2}{8\pi} |V_{cb}|^2 m_{B_c}^2 m_\tau^2 \left(1 - \frac{m_\tau^2}{m_{B_c}^2} \right)^2 f_{B_c}^2 \tau_{B_c} \tag{23}$$

Semileptonic ($\bar{B} \to D^{(*)}\ell\nu_\ell$)

Using a similar approach it is possible to find dependencies for the other observables that consist of semileptonic decays. These are considerably more cumbersome as they will contain hadronic form factors. Hadronic form factors will not be treated in this thesis, for a more complete derivation of the semileptonic dependencies, you can read [**semileptonic functions**]. For simplicity and clarity only the Wilson coefficients treated in the thesis will be written down. The dependencies are taken from [15] and the full expressions with all Wilson coefficients can be found there. In our case $R(D)$ only has contributions from left handed vector operators and its dependency looks like,

$$\begin{aligned}
\mathcal{R}(D)/ \mathcal{R}(D)^{\mathrm{SM}}\Big|_\tau &= \left| 1 + C_{V_L}^{c,\tau} \right|^2 \\
\mathcal{R}(D)/ \mathcal{R}(D)^{\mathrm{SM}}\Big|_{e,\mu} &= \left[0.50 \left| 1 + C_{V_L}^{c,e} \right|^2 + 0.50 \left| 1 + C_{V_L}^{c,\mu} \right|^2 \right]^{-1}
\end{aligned} \tag{24}$$

where the top expression includes the NP effect only in the tau lepton, and the bottom expression for the electron and muon. To get an expression that includes all NP effects, you have to multiply both expressions together.

$R(D^*)$ also has contributions from the pseudoscalar operators and the dependencies look as follows,

$$\begin{aligned}
\mathcal{R}(D^*)/ \mathcal{R}(D^*)^{\mathrm{SM}}\Big|_\tau &= \left| 1 + C_{V_L}^{c,\tau} \right|^2 + 0.11 \left(1 + C_{V_L}^{c,\tau} \right) C_P^{c,\tau} + 0.034 |C_P^{c,\tau}|^2 \\
\mathcal{R}(D^*)/ \mathcal{R}(D^*)^{\mathrm{SM}}\Big|_{e,\mu} &= \Big[0.501 \left| 1 + C_{V_L}^{c,e} \right|^2 + 4.50 \times 10^{-5} \left(1 + C_{V_L}^{c,e} \right) C_P^{c,e} + 0.026 |C_P^{c,e}|^2 \\
&\quad + 0.499 \left| 1 + C_{V_L}^{c,\mu} \right|^2 + 0.009 \left(1 + C_{V_L}^{c,\mu} \right) C_P^{c,\mu} + 0.025 |C_P^{c,\mu}|^2 \Big]^{-1}
\end{aligned} \tag{25}$$

where again the top expression includes only NP effect in the tau lepton and the bottom only for the electron and muon. Like $R(D)$ both expressions can be multiplied with each other to create an expression including all NP effects in the leptons.

Both $F_L(D^*)$ and $R_\mu^e(D^*)$ have contributions from left-handed vector and pseudoscalar operators. Their expesions are

$$F_L\left(D^*\right) = \left(\mathcal{R}\left(D^*\right)^{\mathrm{SM}} / \left.\mathcal{R}\left(D^*\right)\right|_\tau\right) \left[0.46\left|1 + C_{V_L}^{c;\tau}\right|^2 + 0.11\left(1 + C_{V_L}^{c;\tau}\right) C_P^{c;\tau} + 0.034\left|C_P^{c;\tau}\right|^2\right] \quad (26)$$

$$\mathcal{R}_\mu^e\left(D^*\right) / \mathcal{R}_\mu^{e\,\mathrm{SM}}\left(D^*\right) = \frac{|1 + C_{V_L}^{c;e}|^2 + 8.981 \times 10^{-5}\left(1 + C_{V_L}^{c;e}\right) C_P^{c;e} + 0.051\left|C_P^{c;e}\right|^2}{|1 + C_{V_L}^{c;\mu}|^2 + 0.018\left(1 + C_{V_L}^{c;\mu}\right) C_P^{c;\mu} + 0.051\left|C_P^{c;\mu}\right|^2} \quad (27)$$

3.3   Fitting strategy

The Wilson coefficients are constrained in confidence level intervals. By the use of the Gamma-Combo[28] Framework, the Wilson coefficient dependence of the observables, together with their measurements in table 1, construct Probability density functions (PDFs). These PDFs are used to construct a global likelihood function that can find be used to find confidence levels, 68% and 95%, or 1D and or 32% and 87% for 1D or 2D scans, respectively. A more detailed overview can be found in the GammaCombo manual[28]. Within this GammaCombo framework, I have created my own module to combine different measurements of the observables in order to constrain the Wilson coefficients.

As a control, the $B \to D\ell\nu_\ell$ observables are done first and cross-checked with [15].

At first, I assumed only either $C_{V_L}^{c,\ell}$ or $C_P^{c,\ell}$ NP effects. I will also look at the situation where both are considered, where finding bounded constraints could be more cumbersome.

4   Result

This section will present the results from the analysis described in the previous section. First, the $B \to D^{(*)}\ell\nu_\ell$ constraints will be briefly described to gain an understanding of their shapes. Secondly, the constraints given by $\mathcal{B}r(B_c \to \tau\nu_\tau)$ are produced and described. And finally, all observables are used to get new constraints for the pseudoscalar and left-handed vector Wilson coefficients.

4.1 $\mathcal{R}(D^{(*)})$, $\mathcal{R}_\mu^e(D^*)$ and $F_L(D^*)$

This section will introduce the constraints for the $B \to D\ell\nu_\ell$ observables and compare them with [15], Using the updated measurements for $R(D)$, $R(D^*)$ and $F_L(D^*)$. One figure will be shown per Wilson coefficient type. For $C_P^{c,\ell}$ this will be $C_P^{c,\mu} = C_P^{c,e}$(figure 6) and for $C_{V_L}^{c,\ell}$ it is $C_{V_L}^{c,\mu} = 10 C_{V_L}^{c,e}$ (figure 7). The numerical values of the constraints are in tables 3 and 4 and will be combined with the constraints of $\mathcal{B}r(B_c \to \tau\nu_\tau)$
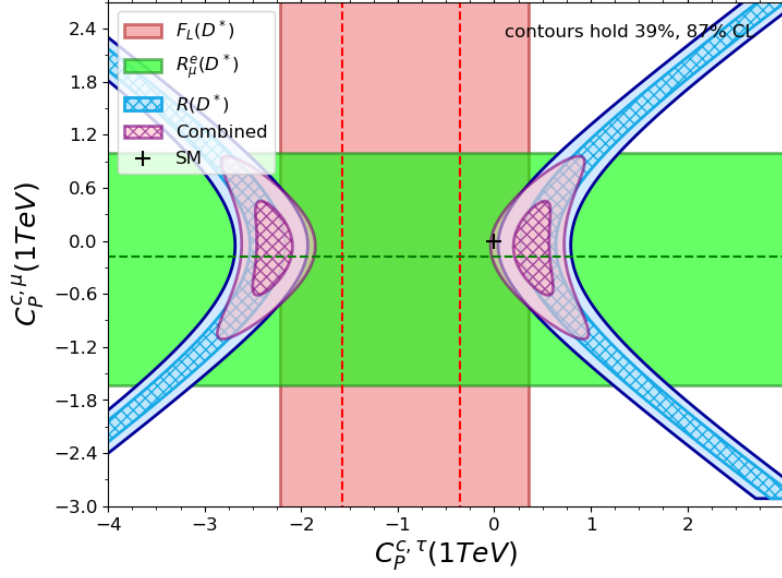
Figure 6: The 3 observables sensitive to the pseudoscalar effective operator, $F_L(D^*)$ (red), $\mathcal{R}^e_\mu(D^*)$ (green) and $\mathcal{R}_{D^{(*)}}$ (blue). The combined fit of all three observables is shown in purple. For this figure $C^{c,e}_P = C^{c,\mu}_P$

Notable is the two central values for $F_L(D^*)$ and only one bound region. This is different in [15] where $F_L(D^*)$ produced two bound region in $C^{c,\tau}_P$. This can be explained by the updated value for $F_L(D^*)$ being closer to the SM value, and therefore the two regions in [15] come closer together to form one bound constraint. There is not enough overlap to create a single central value.

as the other observable measurements did not change much or at all and show nice agreement with the constraints in [15].
Together, the combined constraints create two separate bound regions, one close to the SM and one more negative.
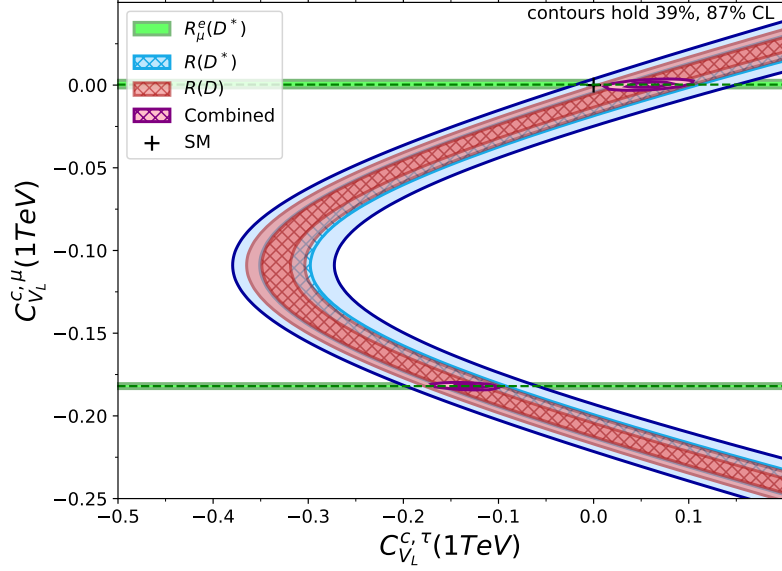
Figure 7: The most positive side of the constraints on C_{V_L} considering the $B \to D\ell\nu_\ell$ observables.

While $F_L(D^*)$ does contribute to $C_{V_L}^{c,\tau}$, when it is the only Wilson coefficient considered, the contributions cancel. $R(D)$ does contribute to $C_{V_L}^{c,\ell}$ unlike with $C_P^{c,\ell}$ and looks like the $R(D^*)$ constraint while having smaller uncertainties.

Figure 7 shows one pair of bound regions closest to the SM value of the Wilson coefficients. There are two more constraints mirrored in $C_{V_L}^{c,\tau} = -1$ to the ones in the figure. Overall, the constraints agree with [15].

4.2 $B_c \to \tau\nu_\tau$

Looking only at the $B_c \to \tau\nu_\tau$ branching fraction to constrain the Wilson coefficients, two bound regions are found (fig 8). Figure 8 also shows that the bound regions are not symmetric around their central value as a consequence of the parabolic shape of the OPE. The intersection between theory and measurement will lead to two disjoint regions. These two regions will create two bands in the following figures.
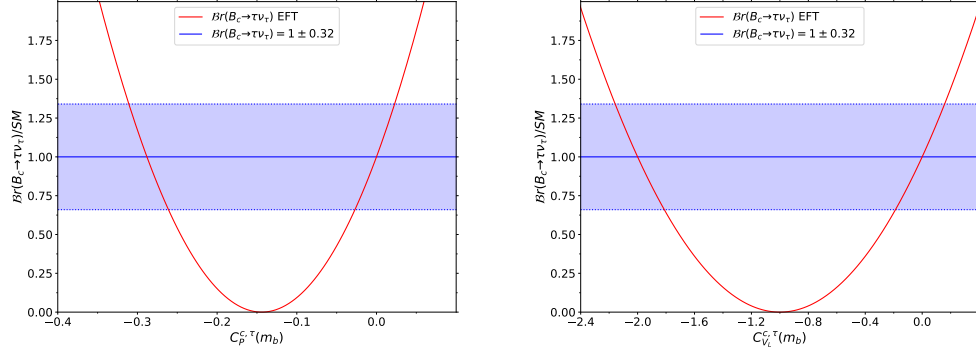

Figure 8: $\mathcal{B}r(B_c \to \tau\nu_\tau)$ as a function of Wilson coefficients(red) and the SM value of the $B_c \to \tau\nu_\tau$ branching fraction with the uncertainty calculated before(blue). Only $C_P^{c,\tau}$ or $C_{V_L}^{c,\tau}$ contributions are assumed in the left and right graphs, respectively. Important to note is that the Wilson coefficients are described at the energy of the decay process.

$C_P^{c,\tau}(1TeV)$	$C_{V_L}^{c,\tau}(1TeV)$
$[-0.313, -0.243]$	$[-2.15, -1.82]$
$[-0.032, 0.027]$	$[-0.18, 0.15]$

Table 2: Numerical results of the $\mathcal{B}r(B_c \to \tau\nu_\tau)$ constraints.

4.2.1 Pseudoscalar

The first assumption is to consider only the NP contribution in the Wilson coefficients of the effective pseudoscalar operator, setting all other contributions to zero. Next to simplify the analysis and reduce fitting parameters, the relation between $C_P^{c,e}$ and $C_P^{c,\mu}$ will be fixed at 3 values, as explained in section 2.3. Each graph in figure 9 contains constraints for 3 different scenarios. — only $B \to D^{(*)}\ell\nu_\ell$ observables (section 4.1), only $\mathcal{Br}(B_c \to \tau\nu_\tau)$ (section 4.2), and one where all associated observables are considered— Table 3 contains the numerical values of the $C_P^{c,\tau}$ constraints.
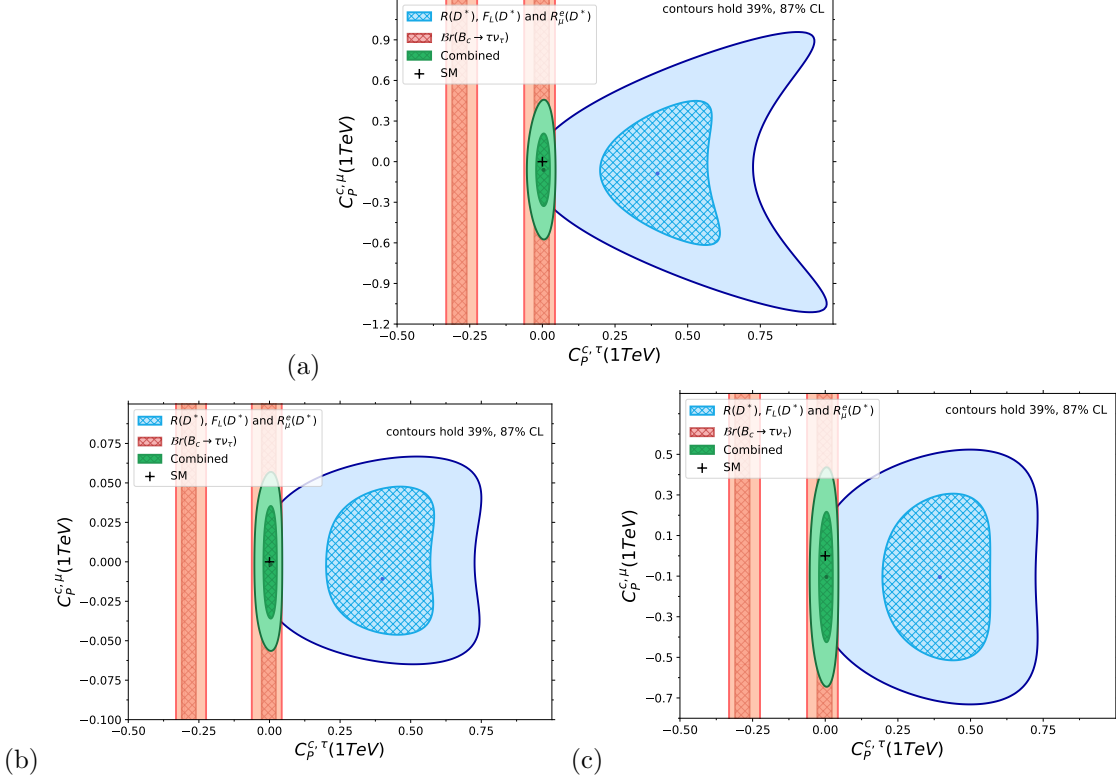

Figure 9: Wilson coefficient constraints of the effective pseudoscalar operator for three different relations between $C_P^{c,e}$ and $C_P^{c,\mu}$. — (a) $C_P^{c,e} = C_P^{c,\mu}$, (b) $C_P^{c,e} = 10C_P^{c,\mu}$, (c) $C_P^{c,e} = 0.1C_P^{c,\mu}$— The blue region represents the constraints of the $B \to D^*\ell\nu_\ell$ observables, red the constraints of $\mathcal{Br}(B_c \to \tau\nu_\tau)$ and the green area is the combination of both the constraints. The best fit value is represented by a dot, and the Standard Model value for the Wilson coefficients is shown using the black cross. Table 3 shows the numerical values of the $C_P^{c,\tau}$ bounds

Figure 9 shows only the positive bound for the $B \to D^{(*)}\ell\nu_\ell$ observables, as to where in section 4.1 two areas were found. The most negative bound for $C_P^{c,\tau}$ together with formula 22 predicts $\mathcal{Br}(B_c \to \tau\nu_\tau)$ to be around 100% or even higher, which is unnatural and thus this region can be discarded (as has also been done in [**AF Esselink**]). The most positive region predicts $\mathcal{Br}(B_c \to \tau\nu_\tau)$ to be between 11% and 43%, which is below the current limit of $\mathcal{Br}(B_c \to \tau\nu_\tau) < 0.60$ [**limBC**]
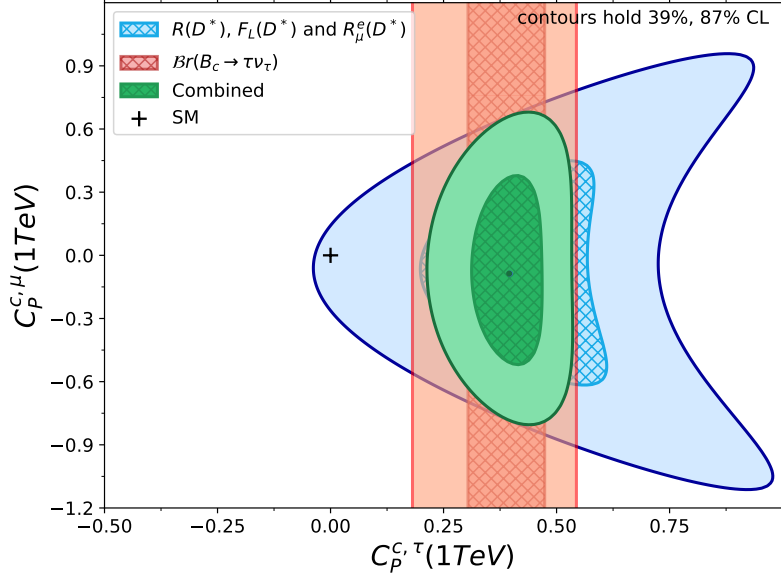
Figure 10: Example of a fit where $\mathcal{Br}(B_c \to \tau\nu_\tau) = 14 \times \mathcal{Br}(B_c \to \tau\nu_\tau)^{SM}$

$\mathcal{Br}(B_c \to \tau\nu_\tau)$ has strong constraining power on $C_P^{c,\tau}$ compared to the other observables, improving the constraint by a factor 6.6. In equations **??** and **??** the factor in front of $C_P^{c,\tau}$ is much smaller than one while the mass ratio in equation 22 is 4.06. This results to the fit converging more to the bounds given by $\mathcal{Br}(B_c \to \tau\nu_\tau)$. In this case, towards the SM value. The combined fit gives one bounded area with uncertainties comparable to $\mathcal{Br}(B_c \to \tau\nu_\tau)$. This result assumes the SM value for $\mathcal{Br}(B_c \to \tau\nu_\tau)$; for higher branching fractions, I assume the uncertainties will increase linearly. For a branching fraction on the central value of the fit in section 4.1 (14 times SM), the uncertainties on the branching fraction are still smaller to those of the $B \to D^{(*)}\ell\nu_\ell$ observables (figure 10).

As $\mathcal{Br}(B_c \to \tau\nu_\tau)$ does not depend on $C_P^{c,\mu}$ and $C_P^{c,e}$ (eq:22), it only indirectly constrains them. In the case $f_\mu^e = 1$ it has the biggest effect, improving the constraint by a factor 2, while for $f_\mu^e = 0.1, 10$ the effect is minimal. Another thing to note is the different scales on the vertical axis in figure 9, as have been noted in section 4.1.

scenario	$C_P^{c,\tau}(1TeV)$		$C_P^{c,\mu}(1TeV)$	
	$B \to D^*\ell\nu_\ell$	combined	$B \to D^*\ell\nu_\ell$	combined
$C_P^{c,e} = C_P^{c,\mu}$	$[-2.503, -2.087]$ $[0.199, 0.611]$	$[-0.020, 0.024]$	$[-0.616, 0.449]$	$[-0.328, 0.209]$
$C_P^{c,e} = 0.1 C_P^{c,\mu}$	$[-2.462, -2.088]$ $[0.197, 0.568]$	$[-0.020, 0.024]$	$[-0.515, 0.306]$	$[-0.425, 0.217]$
$C_P^{c,e} = 10 C_P^{c,\mu}$	$[-2.474, -2.094]$ $[0.201, 0.583]$	$[-0.020, 0.024]$	$[-0.046, 0.047]$	$[-0.036, 0.035]$

Table 3: Numerical results of the pseudoscalar Wilson coefficients for all scenarios. The second and third column showing the tau constraints before and after adding $\mathcal{B}r(B_c \to \tau\nu_\tau)$ to the analysis respectively. The fourth and fifth column showing the corresponding muon constraints.

4.2.2   left-handed vector

In the second scenario considered here, the assumption is that there is only new physics in the left-handed vector operator. I again take the same relations between $C_{V_L}^{c,e}$ and $C_{V_L}^{c,\mu}$ and fit the Wilson coefficients for each case. Figure 11 shows two cases, one where the $\mathcal{B}r(B_c \to \tau\nu_\tau)$ constraint has little effect and one where it creates a bound region. Table 4 shows the numerical values for all bound constraints.
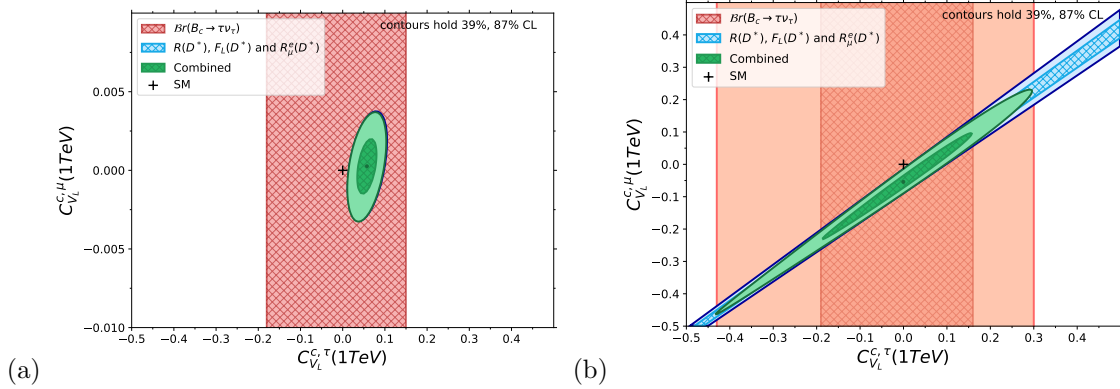

(a)   (b)

Figure 11: Wilson coefficient constraints of the effective left-handed vector operators for two relations between $C_{V_L}^{c,e}$ and $C_{V_L}^{c,\mu}$, — (a) $C_{V_L}^{c,e} = 0.1 C_{V_L}^{c,\mu}$, (b) $C_{V_L}^{c,e} = C_{V_L}^{c,\mu}$— where only the one bound region around the SM value is shown of 4 in each case.

For each relation between $C_{V_L}^{c,e}$ and $C_{V_L}^{c,\mu}$ there are 4 bound regions created by the constraints. As these bound regions are symmetric in $C_{V_L}^{c,\tau} = -1$, figure 11 only shows 2 bounds. While figure 11a assumes $f_\mu^e = 0.1$, the situation for $f_\mu^e = 10$ is very similar, as will be explained in the next paragraph.

When just the $B \to D^{(*)}\ell\nu_\ell$ observables made bound constraints, in the case where $f_\mu^e = 0.1, 10$ as shown in table 4, they are already much smaller than the bound created by $\mathcal{B}r(B_c \to \tau\nu_\tau)$. Figure 11a shows this for one example where the constraint for the $B \to D^{(*)}\ell\nu_\ell$ observables and the

combined constrained overlap for their majority and the $\mathcal{Br}(B_c \to \tau\nu_\tau)$ constraint is much weaker.

When $f_\mu^e = 1$ the $B \to D^{(*)}\ell\nu_\ell$ observables do not a specific central value for $C_{V_L}^{c,\tau}$ and $C_{V_L}^{c,\mu}$. When the constraint on $\mathcal{Br}(B_c \to \tau\nu_\tau)$ is added it is possible to create a bound constraint in the $C_{V_L}^{c,\tau} - C_{V_L}^{c,\mu}$ plane. One thing to note is the 20-fold difference in scale on the vertical axis between figure 11a and 11b. While you do get a bound constraint with the added observable, it is not as strong as where $f_\mu^e = 0.1, 10$.

scenario	$C_{V_L}^{c,\tau}(1TeV)$		$C_{V_L}^{c,\mu}(1TeV)$
	$B \to D^*\ell\nu_\ell$	combined	combined
$C_{V_L}^{c,e} = C_{V_L}^{c,\mu}$	**No bounds**	$[-2.148, -1.826] \cup [-0.174, 0.148]$	$[-2.088, -1.781]$
		$[-2.148, -1.826] \cup [-0.174, 0.148]$	$[-0.219, 0.088]$
$C_{V_L}^{c,e} = 0.1C_{V_L}^{c,\mu}$	$[-1.882, -1.846] \cup [-0.154, -0.118]$	$[-1.883, -1.847] \cup [-0.153, -0.117]$	$[-1.828, -1.805]$
	$[-2.078, -2.032] \cup [0.032, 0.078]$	$[-2.077, -2.031] \cup [0.031, 0.077]$	$[-0.020, 0.015]$
$C_{V_L}^{c,e} = 10C_{V_L}^{c,\mu}$	$[-1.884, -1.848] \cup [-0.152, -0.116]$	$[-1.885, -1.849] \cup [-0.151, -0.115]$	$[-0.183, -0.181]$
	$[-2.082, -2.035] \cup [0.035, 0.082]$	$[-2.080, -2.034] \cup [0.034, 0.080]$	$[-0.001, 0.002]$

Table 4: Numerical results of the left handed vector Wilson coefficients for all scenarios. The second and third column showing the tau constraints before and after adding $\mathcal{Br}(B_c \to \tau\nu_\tau)$ to the analysis. The last column shows the corresponding muon constraint.

4.2.3   Pseudoscalar and Left handed vector

Now I will consider the case where both the pseudoscalar and left-handed vector operator contribute to the observables. In order to keep the DOF manageable and not under constrain the fit, I assume no NP in the muon and electron operators

$$C_P^{c,\mu} = C_P^{c,e} = C_{V_L}^{c,\mu} = C_{V_L}^{c,e} = 0, \tag{28}$$

such that all NP is confined in the tau operator. I believe this assumption is reasonable as these WC in the previous fits are all compatible with 0. Figure 12 shows the results of this fit.
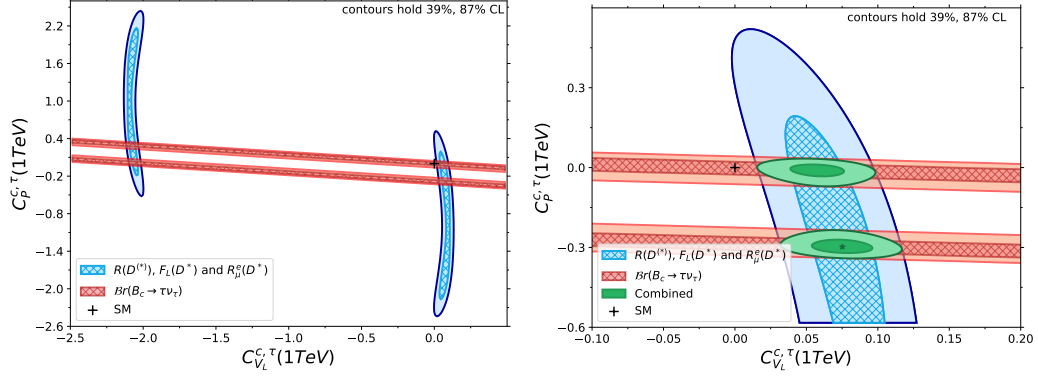
Figure 12: The global scan of $C_P^{c,\tau}$ and $C_{V_L}^{c,\tau}$
(left) and a scan around the SM (right).

In the 2D case, the Pseudoscalar constraint by the $B \rightarrow D\ell\nu_\ell$ observables is much weaker, with a much wider range. Much of this space can already be discarded by imposing the limit $\mathcal{Br}(B_c \rightarrow \tau\nu_\tau) < 0.60$[**limBC**] The vector constraint doesn't change much when contributions from the Pseudoscalar operator are added. There are still 4 bound regions centred around 0 and -2. This does change with the assumption that muons and electrons do not contribute to NP. Without this assumption, it is not possible to secure a bound region as constraints.

The constraints of $B_c \rightarrow \tau\nu_\tau$ creates 2 contours almost orthogonal to the $B \rightarrow D\ell\nu_\ell$ observable constraints. The full constraint is the overlap between them, significantly decreasing the area in the pseudoscalar Wilson coefficient.

While figure 12 only shows the combined constraint close to the SM values of the Wilson coefficients, the other bounds are point symmetric through $(C_{V_L}^{c,\tau}, C_P^{c,\tau}) = (-1, 0)$. This becomes clear by looking at the numerical results in table 5

$B \rightarrow D^*\ell\nu_\ell$		combined	
$C_{V_L}^{c,\tau}(1TeV)$	$C_P^{c,\tau}(1TeV)$	$C_{V_L}^{c,\tau}(1TeV)$	$C_P^{c,\tau}(1TeV)$
$[-2.107, -2.035]$	$[-0.193, 2.167]$	[0.054 , 0.096]	[-0.320 , -0.272]
$[0.035, 0.107]$	$[-2.167, 0.193]$	[0.039 , 0.076]	[-0.031 , 0.011]
		[-2.076 , -2.039]	[-0.011 , 0.031]
		[-2.096 , -2.054]	[0.272 , 0.320]

Table 5: Numerical results for the left handed vector and pseudoscalar Wilson coefficients. The first two and last two columns showing the constraint before and after adding $\mathcal{Br}(B_c \rightarrow \tau\nu_\tau)$ to the analysis respectively.

5 Conclusions

The $b \rightarrow c\ell\nu_\ell$ transition is an interesting probe to test the SM and perhaps even find new physics. I have constrained the NP in the Wilson coefficients, concerning the $b \rightarrow c\ell\nu_\ell$ quark-level transition,

in an Effective Field Theory framework. The following measurements, $R(D^*)$, $R(D)$, $R_\mu^e(D^*)$ and $F_L(D^*)$, are used from the $B \to D\ell\nu_\ell$ and $B \to D^*\ell\nu_\ell$ decays. The SM branching fraction of $B_c \to \tau\nu_\tau$, which LHCb is currently searching for, is added as an observable to find its constraining power. These observables are expanded in the EFT framework to find their Wilson coefficients contributions. Using GammaCombo, these observables together create a constraint in the form of a Confidence Level interval. Either for the pseudoscalar coefficient, the left-handed vector coefficient, or a combination of both. The goal is to find the effect of the added observable $\mathcal{B}r(B_c \to \tau\nu_\tau)$.

The branching fraction for $B_c \to \tau\nu_\tau$ is a great addition for constraining the Pseudoscalar Wilson coefficients. Both in the case where it is the only contribution, as well as when both pseudoscalar and vector contributions are considered. When looking only at NP in the pseudoscalar Wilson coefficients the constraints on these Wilson coefficients improves by a factor 6.6.

For the constraints on the left-handed vector Wilson coefficients, the predicted branching fraction of $B_c \to \tau\nu_\tau$ will not be accurate enough. The current constraints are already more precise than those of the pseudoscalar Wilson coefficients and therefore the effect $B_c \to \tau\nu_\tau$ will have is minimal. An exception is the case where $C_{V_L}^{c,e} = C_{V_L}^{c,\mu}$, where the current $B \to D\ell\nu_\ell$ observables are not able to form a bound region due to the contributions from $R_\mu^e(D^*)$ cancelling, removing a constraint for muons and electrons. In this case, the $B_c \to \tau\nu_\tau$ branching fraction helps create a bound region. I do have to note that this constraint is roughly 6 times larger in the tau coefficient and roughly 100 times larger in the muon and electron coefficients compared to the case where $C_{V_L}^{c,e} \neq C_{V_L}^{c,\mu}$.

It would be interesting to see the interplay with the other Wilson coefficients (the vector right, scalar, and tensor). While they have no contribution to the branching fraction of $B_c \to \tau\nu_\tau$, they can of course be present in other processes and/or decays.

While $R(D)/R(D^*)$ shows an exciting tension with the SM, it alone is not enough to properly constrain NP. It would be great to have more decays to add to this analysis in order to get stronger constraints for the Wilson coefficients. The $B_c \to \tau\nu_\tau$ branching fraction will be a great asset to constrain NP pseudoscalar Wilson coefficients in general. For left-handed vector Wilson coefficients in the case where muon and electron couplings are equal, it is able to find bound constraints where previous observables could not.

References

[1] John Iliopoulos. "The Standard Model". In: *Symposium on the History of the Standard Model*. First comprehensive single-report presentation of the SM. 1974.

[2] Makoto Kobayashi and Toshihide Maskawa. "CP Violation in the Renormalizable Theory of Weak Interaction". In: *Progress of Theoretical Physics* 49 (1973), pp. 652–657. DOI: 10.1143/PTP.49.652.

[3] S.W. Herb, L.M. Lederman, and et al. "Observation of a dimuon resonance at 9.5 GeV in 400-GeV proton-nucleus collisions". In: *Phys. Rev. Lett.* 39 (1977), pp. 252–255.

[4] DØ Collaboration. "Observation of the Top Quark". In: *Phys. Rev. Lett.* 74 (1995), pp. 2632–2637.

[5] CDF Collaboration. "Observation of Top Quark Production in Pbar-P Collisions". In: *Phys. Rev. Lett.* 74 (1995), pp. 2626–2631.

[6] ATLAS Collaboration. "Observation of a new particle in the search for the Standard Model Higgs boson with the ATLAS detector at the LHC". In: *Phys. Lett. B* 716 (2012), pp. 1–29.

[7] CMS Collaboration. "Observation of a new boson at a mass of 125GeV with the CMS experiment at the LHC". In: *Phys. Lett. B* 716 (2012), pp. 30–61.

[8] Vera C. Rubin and W. Kent Jr. Ford. "Rotational properties of M31 and implications for unseen mass". In: *Astrophys. J.* 159 (1970), pp. 379–403.

[9] R. Aaij and et al. (LHCb Collaboration). "Measurement of the ratio of branching fractions $\mathcal{B}(\bar{B}^0 \to D^{*+}\tau^-\bar{\nu}_\tau)/\mathcal{B}(\bar{B}^0 \to D^{*+}\mu^-\bar{\nu}_\mu)$". In: *Phys. Rev. Lett.* 115.11 (2015), p. 111803. arXiv: 1506.08614.

[10] M. Huschle and et al. (Belle Collaboration). "Measurement of the branching ratio of $\bar{B} \to D^{(*)}\tau^-\bar{\nu}_\tau$ relative to $\bar{B} \to D^{(*)}\ell^-\bar{\nu}_\ell$ decays with hadronic tagging at Belle". In: *Phys. Rev. D* 92 (2015), p. 072014. arXiv: 1507.03233.

[11] J. P. Lees and et al. (BaBar Collaboration). "Measurement of an excess of $B \to D^{(*)}\tau\nu$ decays and implications for charged Higgs bosons". In: *Phys. Rev. D* 88 (2013), p. 072012. arXiv: 1303.0571.

[12] HFLAV Collaboration. *Preliminary world average of $\mathcal{R}(D)$ and $\mathcal{R}(D^*)$*. HFLAV summary (Winter/Summer 2023). World averages: $R(D) = 0.357 \pm 0.029$, $R(D^*) = 0.284 \pm 0.012$. 2023.

[13] CMS Collaboration. "Search for t-channel scalar and vector leptoquark exchange in high-mass dilepton spectra". In: *JHEP* 2024.05 (2024). Excludes LQ masses up to 5TeV at 95% CL (coupling dependent), p. 311. arXiv: 2503.20023.

[14] ATLAS Collaboration. *Search for third-generation leptoquarks decaying to $b\tau$ or $t\ell$*. ATLAS Physics Briefing (based on 139fb^{-1} at 13TeV). Excludes vector LQ masses below 1.75–2.0TeV and scalar LQ→t below 1.64TeV. 2023.

[15] Robert Fleischer, Ruben Jaarsma, and Gilberto Tetlalmatzi-Xolocotzi. "Mapping out the space for new physics with leptonic and semileptonic $B_{(c)}$ decays". In: *The European Physical Journal C* 81.7 (July 2021). ISSN: 1434-6052. DOI: 10.1140/epjc/s10052-021-09419-8. URL: http://dx.doi.org/10.1140/epjc/s10052-021-09419-8.

[16] OpenAI. *GPT-4 Technical Report*. https://openai.com/research/gpt-4. Accessed via ChatGPT with GPT-4-turbo (Plus-abonnement), juli 2025. 2024.

[17] Nicola Cabibbo. "Unitary Symmetry and Leptonic Decays". In: *Physical Review Letters* 10.12 (1963), pp. 531–533. DOI: 10.1103/PhysRevLett.10.531.

[18] Makoto Kobayashi and Toshihide Maskawa. "CP-Violation in the Renormalizable Theory of Weak Interaction". In: *Progress of Theoretical Physics* 49.2 (1973), pp. 652–657. DOI: 10.1143/PTP.49.652.

[19] Y. Aoki et al. "FLAG Review 2024". In: (Nov. 2024). arXiv: 2411.04268 [hep-lat].

[20] Enrico Fermi. "Tentativo di una teoria dell'emissione dei raggi beta". In: *Il Nuovo Cimento (1924-1942)* 11 (1934), pp. 1–19. DOI: 10.1007/BF02959820.

[21] S. Navas et al. "Review of particle physics". In: *Phys. Rev.* D110.8 (2024), p. 030001. DOI: 10.1103/PhysRevD.110.030001.

[22] Syuhei Iguro, Michihisa Takeuchi, and Ryoutaro Watanabe. "Testing leptoquark/EFT in

$$\bar{B} \to D^{(*)} l \bar{\nu}$$

at the LHC". In: *The European Physical Journal C* 81.5 (May 2021). ISSN: 1434-6052. DOI: 10.1140/epjc/s10052-021-09125-5. URL: http://dx.doi.org/10.1140/epjc/s10052-021-09125-5.

[23] LHCb collaboration R. Aaij et al. *Measurement of the D^* longitudinal polarization in $B^0 \to D^{*-} \tau^+ \nu_\tau$ decays.* 2023. arXiv: 2311.05224 [hep-ex]. URL: https://arxiv.org/abs/2311.05224.

[24] Belle Collaboration, A. Abdesselam, et al. *Measurement of the D^{*-} polarization in the decay $B^0 \to D^{*-} \tau^+ \nu_\tau$.* 2019. arXiv: 1903.03102 [hep-ex]. URL: https://arxiv.org/abs/1903.03102.

[25] Maria Domenica Galati. "Phd to be submitted". In: ().

[26] Y. Amhis et al. "Averages of b-hadron, c-hadron, and τ-lepton properties as of 2021". In: *Phys. Rev.* D107 (2023). updated results and plots available at https://hflav.web.cern.ch, p. 052008. DOI: 10.1103/PhysRevD.107.052008. arXiv: 2206.07501 [hep-ex].

[27] E. Waheed et al. "Measurement of the CKM matrix element $|V_{cb}|$ from $B^0 \to D^{*-} l^+ \nu_l$ at Belle". In: *Physical Review D* 100.5 (Sept. 2019). ISSN: 2470-0029. DOI: 10.1103/physrevd.100.052007. URL: http://dx.doi.org/10.1103/PhysRevD.100.052007.

[28] Matthew W. Kenzie et al. *GammaCombo User Manual, version 2.1.* Tech. rep. Available at https://gammacombo.github.io/manual.pdf. CERN / University of Cambridge / TU Dortmund, Aug. 2019.